Nanoscale Systems for Optical Quantum Technologies

Grant Agreement No: 712721
Start Date: 1st October 2016 - Duration: 36 months

D3.5 Comparison between FIB samples and thin films for nanoresonators

Deliverable:	D3.5
Work package:	WP3 Opto-electrical and opto-mechanical hybrid systems
Task:	3.3 Eu3+ nano-mechanical oscillators
Lead beneficiary:	CNRS
Type:	Report
Dissemination level:	Public
Due date:	31 September 2018
Actual submission date:	29 December 2018
Author(s):	D. Serrano, P. Goldner (CNRS-CP)

This project has received funding from the European Union's Horizon 2020 research and innovation programme under grant agreement No 712721.

Version history

Version	Date	Author(s)	Description
V1	26/12/2018	D. Serrano, P. Goldner, (CNRS-CP)	Draft
V2	29/12/2018	D. Serrano, P. Goldner, (CNRS-CP), S. Seidelin (CNRS-IN)	Submitted version

Table of Contents

Deliverable Description

In this deliverable, we discuss the choice between focussed ion beam (FIB) fabricated Y_2SiO_5 resonators and Atomic Layer Deposition (ALD) grown Y_2O_3 thin films for the optomechanics experiments that are planned in WP3, Task 3.4: "Coupling of energy levels of Eu^{3+} ions to the vibrations of the nanoscale mechanical oscillator via material strain".

Introduction

In the search of optimum rare-earth systems for optomechanics two alternative approaches have been pursued in NanOQTech: FIB fabrication of resonators from bulk rare-earth (RE) crystals and growth of rare-earth doped thin films on Si substrate. Fabrication of both FIB resonators and thin films have been achieved and reported in Deliverable D3.1: *Nano-resonators* and D1.4: *Optimized particles and thin films*. At this point of the project, it is necessary to choose the most promising system for the next opto-mechanical experiments. This relies primarily on the spectroscopic properties exhibited by the RE dopants in each case. With respect to FIB resonators, research works have shown that bulk optical homogeneous linewidths can be preserved at the nanoscale after FIB processing of RE crystals [1,2]. In contrast, the homogeneous linewidth of trivalent RE in thin films have shown very broad lines with homogeneous widths in the range 10-100 MHz [3,4]. We attempt here the measurement of the optical homogeneous linewidth of Eu^{3+} in an Y_2O_3 thin film grown by ALD. Spectral hole burning (SHB) was used as the characterization technique as it is able to provide insight into hyperfine level lifetimes (T_1) and optical homogenous linewidths (Γ_h).

Methods

Investigated samples and experimental setup

A series of fluorescence-detection based SHB experiments were applied to an ALD grown Y_2O_3:Eu^{3+} thin film (5% at.) with a thickness of 255 nm, after a post-deposition thermal annealing treatment at 950 °C. This temperature was found to maximize the cubic phase contribution with respect to the monoclinic phase in the ALD grown Y_2O_3 films. More details about the ALD method and optimized deposition conditions can be found in Deliverable D1.4: *Optimized particles and thin films*. The same experiments were carried out in a Czochralski grown Eu^{3+} doped Y_2SiO_5 single crystal (0.1%Eu^{3+} and 0.5 mm thick), used here as a reference sample.

The excitation of the Eu^{3+} transition at 580 nm ($^7F_0 \rightarrow {}^5D_0$), was performed by a tunable dye laser with 200 kHz linewidth (Sirah Matisse DS). The continuous laser output was modulated by a double pass AOM with a central frequency of 200 MHz driven by an arbitrary waveform generator (AWG) to create sequences of pulses. Focusing of the excitation beam into the sample and fluorescence collection was carried out, inside a He bath cryostat (Janis SVT-200), by an aspheric lens with 0.77 numerical aperture and 3.1 mm focal length. The position of the lens regarding the sample was optimized to maximize fluorescence collection with an Attocube translation stage (ANPx51/LT). Before detection, the Eu^{3+} $^5D_0$ fluorescence emissions, which peak around 610 nm, were sharply separated from the excitation wavelength by a dichroic mirror and several fluorescence filters located along the collection path. An avalanche photodiode (APD Thorlabs 110

A/M) and a high sensitivity photomultiplier tube (PMT Hamamatsu R5108) connected to a 10^6 V/A transimpedance amplifier were used for fluorescence detection in the case of the Y_2SiO_5 crystal and Y_2O_3 thin film respectively. The fluorescence signal from the crystal was indeed too large for the high sensitivity PMT, which was nevertheless very suitable for the thin film. The detected fluorescence intensity was displayed on a digital oscilloscope together with the excitation laser pulses collected by the reference diode (PDA 10A-EC).

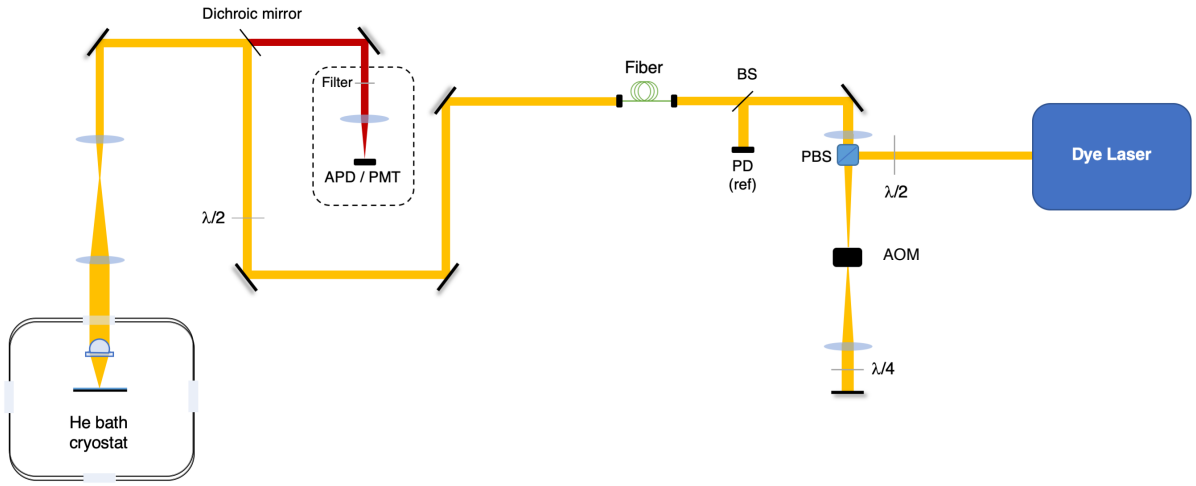

Figure 1: Low temperature fluorescence microscopy setup. BS and PBS stand for beam splitter and polarizing beam splitter respectively; PD for photodiode; APD for avalanche photodiode and PMT for photomultiplier tube. Half-wave plates were used to rotate the linear polarization direction.

SHB sequences

Spectral holes in RE doped crystals are most often experimentally evidenced by the increase in transmission of a laser probe at the burn frequency [5]. When transmission is monitored in conditions of weak excited state population, the holes are due to the redistribution of population between ground state hyperfine levels induced by the burn pulse. This laser transmission-based method, extensively applied to bulk crystals, is more difficult to use with nanometer-thick films deposited on an opaque substrate, such as our ALD Y_2O_3:Eu^{3+} on silicon samples. For this reason, an alternative scheme for SHB investigations was developed using the low-temperature fluorescence microscopy excitation and collection configuration described in the previous section (**Figure 1**). When dealing with very low optical densities, detecting fluorescence can be very advantageous. Indeed, fluorescence from RE ions has intrinsic spectral and dynamical features (narrow lines, long excited state lifetime) that allows discriminating it against background signals. In addition, a microscopy configuration is the most suitable for efficient excitation and collection of emission from small volumes.

Three different fluorescence-detection based SHB sequences were tested in the Y_2SiO_5:Eu^{3+} crystal and the Y_2O_3:Eu^{3+} film, hereinafter referred to as *burn-probe* (**Fig. 2a**), *burn-scan* (**Fig. 2b**) and *three-frequencies* (**Fig. 2c**). In the *burn-probe* sequence, a spectral hole created by a burn pulse at frequency ν is evidenced by the contrast in fluorescence emission generated by a short probe pulse at a fixed frequency $\nu+\delta\nu$, when the sequence

is repeated for different values of δν around δν=0 (**Fig. 2a**). The replacement of this probe by a weak frequency-chirped pulse to map the spectral hole corresponds to the *burn-scan* sequence (**Fig. 2b**). The *three-frequencies* sequence (**Fig. 2c**), a bit more complex than the two previous ones, consists in burning at two different laser frequencies, ν_1 and ν_2, with ν_1 - ν_2 matching one of the Eu^{3+} ground state hyperfine transitions (see the example in **Figure 3**). A short readout pulse is then tuned to a third frequency ν_3, corresponding to a transition from the ground state hyperfine level not pumped in the previous step and which is therefore expected to exhibit population excess (anti-hole). All sequences are ended up by population re-initialization to thermal equilibrium by a series of strong and broadband chirped pulses (*Repump*).

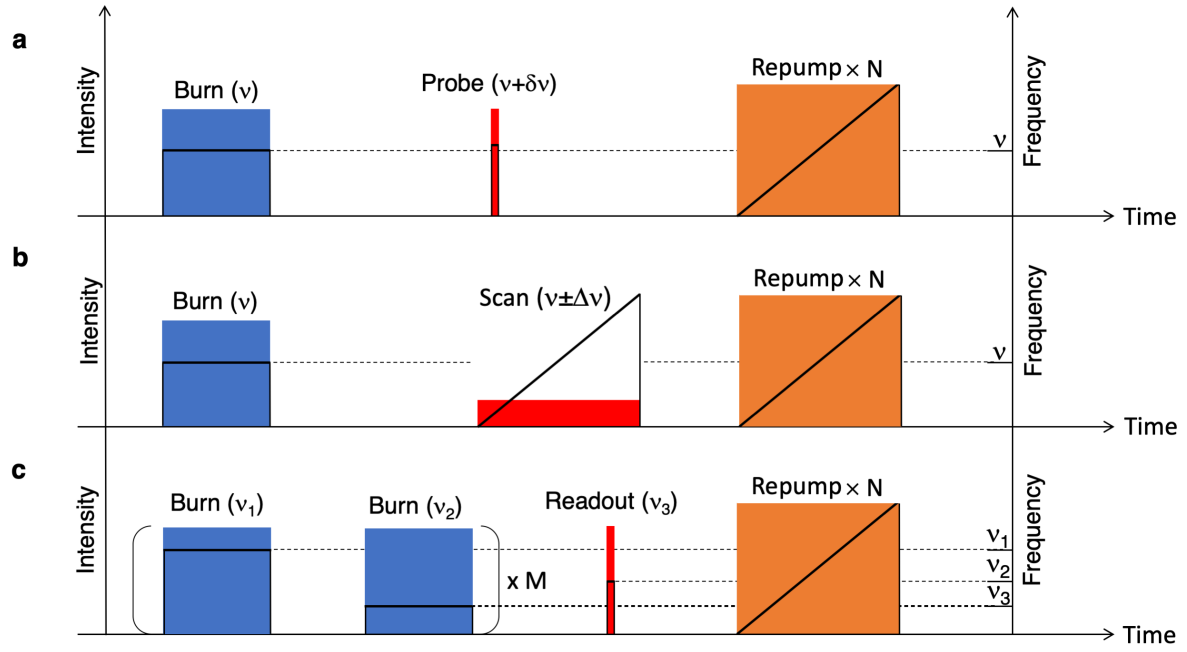

Figure 2: Fluorescence-detection based spectral hole burning sequences. **a.** Burn-probe sequence. **b.** Burn-scan sequence. **c.** Three frequencies sequence. The left axis refers to pulse intensity and the right axis to pulse frequency.

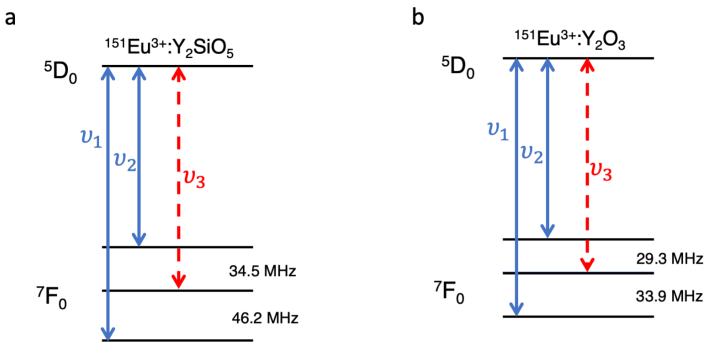

Figure 3: Detail of the pumping and probing frequencies used in the *three-frequencies* sequence when applied to **a.** $^{151}Eu^{3+}:Y_2SiO_5$ and **b.** $^{151}Eu^{3+}:Y_2O_3$.

Results

The fluorescence response of the Y_2O_3 film and reference Y_2SiO_5 crystal is displayed in **Figure 4** for pulses of 5 ms and 10 ms respectively. In both cases, the excitation power was set to 50 mW. As observed, around 2 ms of excitation is required to reach steady-state emission. In the Y_2SiO_5:Eu^{3+} case, the fluorescence emission intensity starts to decrease shortly afterwards due to SHB starting to take place. No such effect is however observed in the case of the Y_2O_3 thin film regardless of the pumping time (e.g. 10 ms instead of 5 ms). The characteristic fluorescence decay from the Eu^{3+} $^5D_0$ level can be observed at the end of the excitation pulse. Optical T_1 of 1.7 ms and 850 µs were estimated by single-exponential fit for the Y_2SiO_5: 0.1%Eu^{3+} crystal and Y_2O_3: 5%Eu^{3+} film respectively. A fast luminescence decay component (a few µs) was also observed in the case of the film and was attributed to background fluorescence from the silicon substrate.

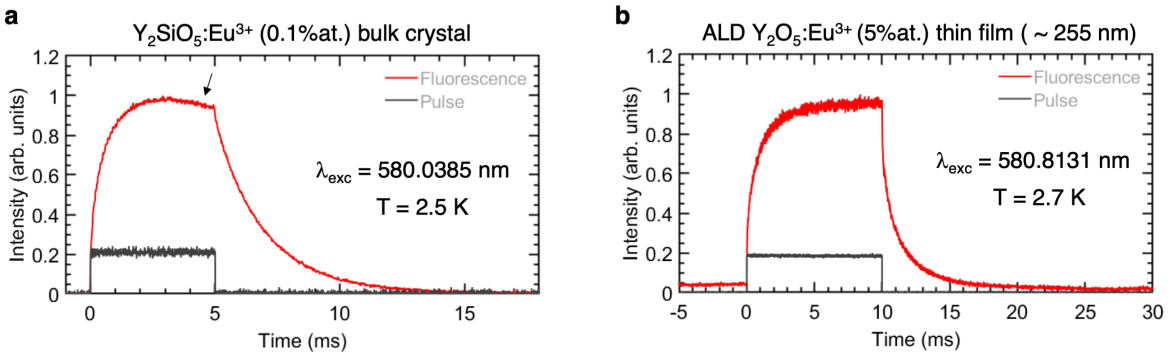

Figure 4: Fluorescence response to a single excitation pulse in **a.** Eu^{3+}:Y_2SiO_5 and **b.** Eu^{3+}:Y_2O_3 film. A decrease in fluorescence emission intensity is observed in Eu^{3+}:Y_2SiO_5 as the optical pumping takes place.

The fluorescence intensity decrease due to SHB can be clearly observed in Y_2SiO_5:Eu^{3+} in **Figure 5**, which contrasts with the Y_2O_3:Eu^{3+} film, where no effect is detected.

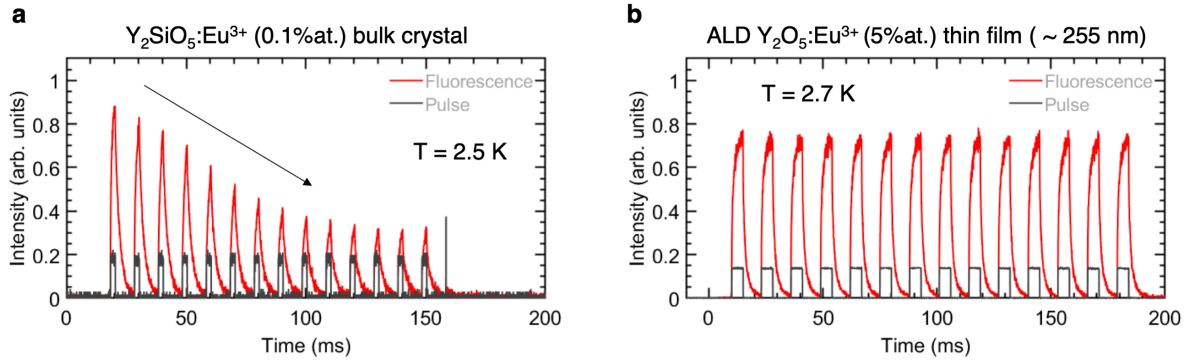

Figure 5: Fluorescence response to a train of pulses, all with the same excitation frequency corresponding to the center of the inhomogeneous absorption line in **a.** Eu^{3+}:Y_2SiO_5 and **b.** Eu^{3+}:Y_2O_3 film.

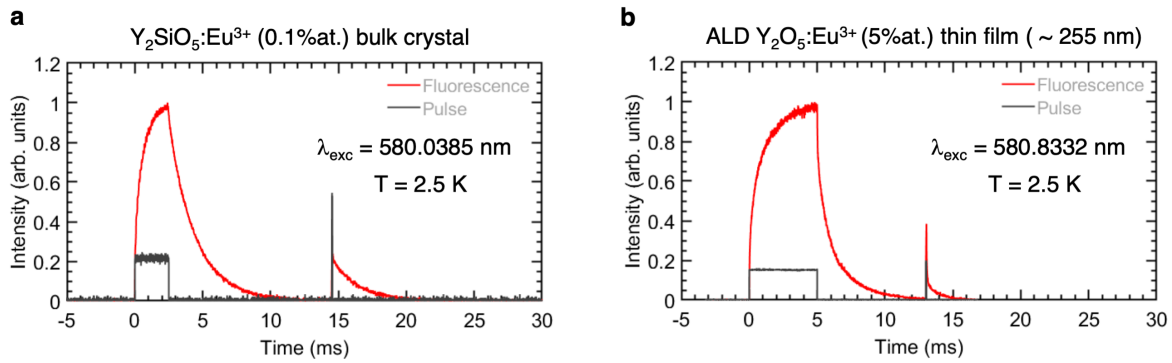

Figure 6: Fluorescence and laser intensity traces for the burn-probe sequence applied to **a.** $Eu^{3+}:Y_2SiO_5$ and **b.** $Eu^{3+}:Y_2O_3$ film. The fluorescence decay integrated intensity after the probe pulse was monitored as a function of the probe pulse detuning with respect to the pump.

After preliminary adjustment of the length of the burning pulses and that of the minimum delay between two pulses to avoid any addition of their respective fluorescence decays, the three SHB sequences in **Figure 2** where applied. An example of the recorded traces resulting from the *burn-probe* sequence is shown in **Figure 6**. No fluorescence contrast, indicating the occurrence of SHB could be observed in the $Y_2O_3:Eu^{3+}$ film for any of the sequences. The conclusion was very different in the case of the $Y_2SiO_5:Eu^{3+}$ reference sample since all sequences showed clear evidence of SHB (**Figs. 7 and 8**).

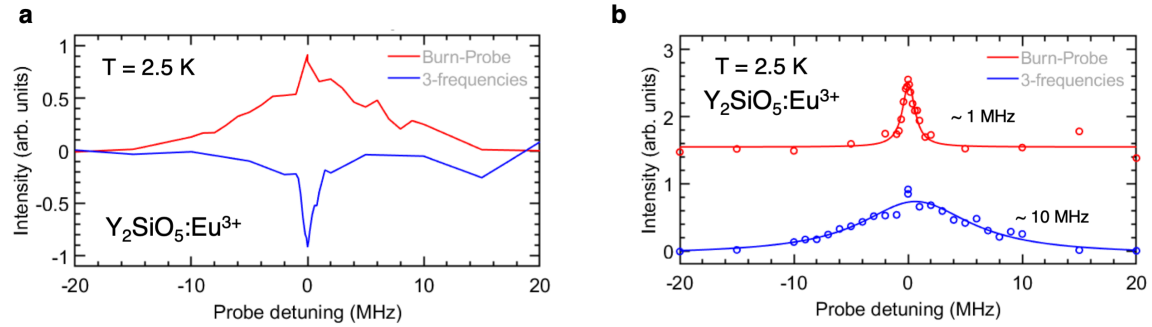

Figure 7: Fluorescence contrast resulting from the burn-probe and three-frequencies sequences when detuning the probe/readout pulse. **a.** The burn-probe measurement yields a hole while an anti-hole is measured by the three-frequencies sequence **b.** Lorentzian fit of the hole and anti-hole in a.

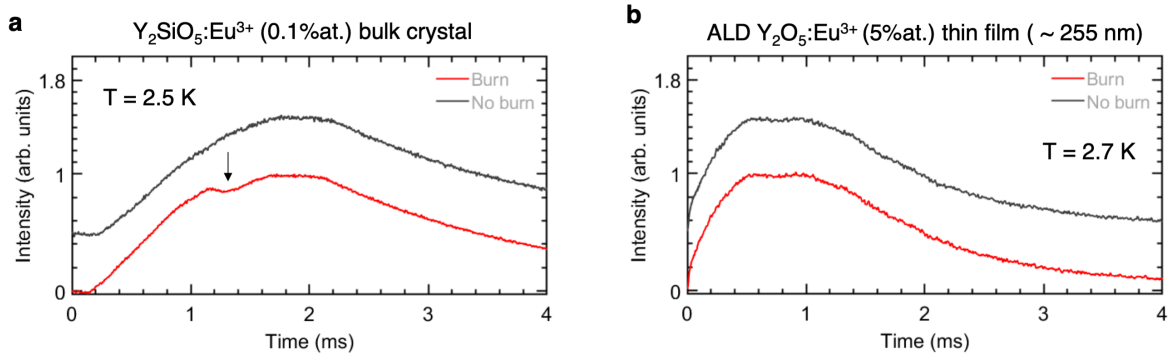

Figure 8: Fluorescence response to the scan pulse in the burn-scan sequence when switching the burn pulse on (red line) and off (black line) for **a.** $Eu^{3+}:Y_2SiO_5$ and **b.** $Eu^{3+}:Y_2O_3$ film. A difference between the burn and no burn cases is only observed for the $Eu^{3+}:Y_2SiO_5$ sample.

Discussion

Fluorescence contrasts resulting from SHB were rather straightforwardly detected in the reference Y_2SiO_5:Eu^{3+} sample by the three sequences investigated. This was not the case in the thin film where no evidence of SHB could be observed. This cannot be attributed to a fluorescence collection efficiency issue since very good fluorescence signal to background and signal to noise ratios could be achieved in the film. We therefore conclude that SHB does not occur in the film. This can be due to a too short hyperfine T_1 (< 1-5 ms), allowing the holes to relax before detection. Indeed, the methods we used are not suitable to probe spectral holes at time delays shorter than the Eu^{3+} fluorescence decay time. This can be considered as a disadvantage of the fluorescence-detection approach with respect to the transmission approach. Reduced hyperfine lifetimes can be due to magnetic defects and have been observed in RE doped nanoparticles and transparent ceramics [6],[7]. Another problem when investigating ALD thin films is the presence of both cubic and monoclinic phases in the sample (see D1.4). Even when we chose the excitation wavelength to meet the maximum absorption of the cubic phase, the monoclinic phase emission is also excited, because of the broad absorption associated with this unwanted phase. The monoclinic phase emission therefore gives rise to an unavoidable background, which potentially masks any fluorescence contrast due to SHB in the cubic phase. Indeed, the very broad emission of the monoclinic phase (~1000 GHz) suggests the presence of a high concentration of defects that are likely to reduce hyperfine lifetimes

With respect to the three florescence-detection sequences we used for SHB investigations, the *burn-probe* sequence stands out as the one providing the better fluorescence contrast and the narrower spectral hole. The hole width measured in this sequence is about 1 MHz, which is in agreement with the values measured on Eu^{3+}:Y_2SiO_5 samples in transmission on our setup. It is dominated by laser jitter and power broadening, since the homogeneous linewidth in Eu^{3+}:Y_2SiO_5 is < 1 kHz, as measured by two-pulse photon echoes [8]. The origin of the much larger widths of the holes measured by the 3-frequencies method is still under investigation but could be related to laser stability issues since the three-frequencies sequence was about 4 times longer than the burn-probe one. The lower contrast resulting from the three-frequencies sequence is not surprising since it results from an antihole (involving a smaller subset of ions). The analysis of the burn-scan result appears less clear because of the interplay between the excitation frequency scan and the long-lived emission that prevent observing ions in a well-defined frequency class.

Conclusion

Current ALD grown films do not exhibit spectral hole burning, which make them unsuitable for the experiments planned in Task 3.4. We will therefore use samples obtained from bulk crystals by FIB for this purpose (D3.1). Results from the literature indicate that bulk properties should be very well preserved in these samples, making them very promising for observing opto-mechanical effects in rare earth doped nano-resonators.

References

1. T. Zhong, J. M. Kindem, E. Miyazono, and A. Faraon, "Nanophotonic coherent light-matter interfaces based on rare-earth-doped crystals," Nat. Commun. **6**, 8206 (2015).
2. T. Zhong, J. M. Kindem, J. G. Bartholomew, J. Rochman, I. Craiciu, E. Miyazono, M. Bettinelli, E. Cavalli, V. Verma, S. W. Nam, F. Marsili, M. D. Shaw, A. D. Beyer, and A. Faraon, "Nanophotonic rare-earth quantum memory with optically controlled retrieval," Science **357**, 1392–1395 (2017).
3. K. Jang and R. S. Meltzer, "Homogeneous and inhomogeneous linewidths of Eu3+ in disordered crystalline systems," Phys. Rev. B **52**, 6431–6439 (1995).
4. H. Liu, G. K. Liu, S. T. Li, J. V. Beitz, and F. E. Fernandez, "Nonlinear optical dynamics and Eu3+ spectral holeburning in strontium barium niobate thin film grown by pulsed laser deposition," J. Appl. Phys. **91**, 129 (2001).
5. R. S. Meltzer, "Line Broadening Mechanisms and Their Measurement," in *Spectroscopic Properties of Rare Earths in Optical Materials*, B. Jacquier and G. Liu, eds. (Springer, 2005), pp. 191–265.
6. N. Kunkel, A. Ferrier, C. W. Thiel, M. O. Ramírez, L. E. Bausá, R. L. Cone, A. Ikesue, and P. Goldner, "Rare-earth doped transparent ceramics for spectral filtering and quantum information processing," APL Mater. **3**, 096103–7 (2015).
7. D. Serrano, J. Karlsson, A. Fossati, A. Ferrier, and P. Goldner, "All-optical control of long-lived nuclear spins in rare-earth doped nanoparticles," Nat. Commun. **9**, 2127 (2018).
8. N. Kunkel, J. Bartholomew, S. Welinski, A. Ferrier, A. Ikesue, and P. Goldner, "Dephasing mechanisms of optical transitions in rare-earth-doped transparent ceramics," Phys. Rev. B **94**, 184301 (2016).